Initial-Rate Kinetics of Human NMN-Adenylyltransferases: Substrate and Metal Ion Specificity, Inhibition by Products and Multisubstrate Analogues, and Isozyme Contributions to NAD^+ Biosynthesis†

Leonardo Sorci,‡ Flavio Cimadamore,‡ Stefania Scotti,‡ Riccardo Petrelli,§ Loredana Cappellacci,§ Palmarisa Franchetti,§ Giuseppe Orsomando,‡ and Giulio Magni*,‡

Istituto di Biotecnologie Biochimiche, Università Politecnica delle Marche, Via Ranieri 67, 60131 Ancona, Italy, and Dipartimento di Scienze Chimiche, Università di Camerino, 62032 Camerino, Italy

Received November 13, 2006; Revised Manuscript Received January 16, 2007

ABSTRACT: Initial-rate and product inhibition studies revealed distinctive ordered ternary complex kinetic mechanisms, substrate specificities, and metal ion preferences for the three isozymes of human nicotinamide mononucleotide adenylyl-transferase (NMNAT, EC 2.7.7.1). ATP binds before NMN with nuclear isozyme NMNAT1 and Golgi apparatus NMNAT2, but the opposite order is observed with the mitochondrial isozyme NMNAT3. Only the latter utilizes ITP efficiently in place of ATP, and while NMNH conversion to NADH by NMNAT1 and NMNAT3 occurs at similar rates, conversion by NMNAT2 is much slower. These isozymes can also be discriminated by their action on tiazofurin monophosphate (TrMP), a metabolite of the antineoplastic prodrug tiazofurin. Our finding that TrMP is only a substrate with NMNAT1 and NMNAT3 reveals for the first time an organelle selectivity in the metabolism of this important drug. In search of additional ways to discriminate these isozymes, we synthesized and tested the P^1-(nicotinamide/nicotinate-riboside-5′)-P^n-(adenosine-5′) dinucleotides Np_3AD, Np_4AD, and Nap_4AD. In addition to being highly effective inhibitors, these multisubstrate geometric inhibitors gave inhibition patterns that are consistent with the aforementioned isozyme differences in substrate binding order. Distinctive differences in their substrate specificity and metal ion selectivity also permitted us to quantify individual isozyme contributions to NAD^+ formation in human cell extracts.

Mounting evidence attests to the paramount importance of the nonredox functions for NAD^+, including its role as a substrate in posttranslational covalent modifications of key proteins, especially mono- and poly-ADP-ribosylation reactions (*1*). Activation of poly(ADP-ribose) polymerase plays a decisive role in NAD^+ depletion and concomitant processes resulting in cell death (*2*). Maintenance of an adequate supply of NAD^+ is also essential for the synthesis of such signaling molecules as cyclic ADP-ribose and $NaADP^+$, potent mobilizers of intracellular Ca^{2+} pools via distinct signaling pathways (*3*). The poly(ADP-ribose) polymerase tankyrase plays an indispensable role in genome integrity by maintaining telomere-length homeostasis (*4*, *5*). NAD^+ is also an essential nonredox cofactor in histone/protein deacetylation catalyzed by a newly recognized deacetylase in the silent information regulator (or SIR2) family (*6*). This discovery suggests that gene silencing might be related to the cellular metabolic rate and that cellular NAD^+ concentrations are directly correlated to a longer cell lifespan. That the human SIR2-homologue SIRT1 acts as a NAD^+-dependent p53 deacetylase raises intriguing questions about aging and cancer (*7*, *8*).

NAD^+ homeostasis is related to the free radical mediated production of reactive oxygen species responsible for irreversible cellular damage in atherosclerosis and neurodegenerative syndromes (*9*). Because the cellular redox status depends on both the absolute concentration of pyridine dinucleotides and their respective ratios of oxidized and reduced forms (i.e., NAD^+/NADH and $NADP^+$/NADPH), it is conceivable that an altered regulation of the synthesis and degradation of NAD^+ impairs the redox state of the cell and likely contributes to the mechanisms underlying the pathogenesis of the above-mentioned diseases. These considerations underscore the imperative for understanding how cells control their intracellular stores of pyridine dinucleotides. Among the routes involved in NAD^+ metabolism, catalysis of NAD^+ formation from NMN and ATP by nicotinamide mononucleotide adenylyltransferase (NMNAT, EC 2.7.7.1) is thus of enduring interest, with respect to both its mechanism and its key regulatory properties (*10*). Equally important are the observations on the NMNAT-mediated synthesis of NAD^+ analogues, and on its implication in chemotherapy. Indeed, injection of acetylpyridine into mouse tumors resulted in the formation of the acetylpyridine analogue of NAD^+ and concomitant reduction of NAD^+ concentration (*11*, *12*). Furthermore, the mechanism underlying the remarkable effect of 6-mercaptopurine in limiting

† This work was supported by Ministero dell'Università e della Ricerca, Italy, PRIN 2004.

* Address all correspondence and inquiries to this author. Mailing address: Istituto di Biotecnologie Biochimiche, Universitá Politecnica delle Marche, Via Ranieri 67, 60131 Ancona, Italy. Tel: +39 071 220 4678. Fax: +39 071 220 4677. E-mail: g.magni@univpm.it.

‡ Universitá Politecnica delle Marche.

§ Università di Camerino.

10.1021/bi6023379 CCC: $37.00
Published on Web 04/03/2007

tumor cell growth has been related to the ability of 6-mercaptopurine riboside triphosphate to competitively inhibit NMNAT, thereby reducing the concentration of NAD^+ to below that required for survival (*13*, *14*). Finally, NMNAT catalyzes the metabolic activation of antineoplastic compounds such as tiazofurin and benzamide riboside, and sufficient NMNAT activity is needed to achieve therapeutic efficacy and to overcome tiazofurin resistance observed in certain tumor cell lines (*15*−*17*). Collectively, these observations indicate NMNAT as a key enzyme for NAD^+ biosynthesis and an interesting target for chemotherapy.

In eukaryotes, NMNAT exists in multiple forms localized in different subcellular compartments (*18*−*22*). In humans, in addition to the well-studied nuclear isozyme NMNAT1, two additional isozymes, NMNAT2 and NMNAT3, have been identified and characterized (*23*). NMNAT2 is localized in the Golgi complex, and NMNAT3 in mitochondria (*24*, *25*). These enzymes exist in different oligomeric states (*24*, *26*), with NMNAT1 a hexamer, NMNAT3 a tetramer, and NMNAT2, whose 3D structure has yet to be determined, behaving as a monomer (*27*). Previous results on the enzyme catalytic properties revealed differences in their substrate specificities and kinetic parameters (*24*, *25*, *27*). However, because there are no effective inhibitors for NMNAT activity, we designed, synthesized, and analyzed several geometric oligophosphate-containing NAD^+ analogues as NMNAT inhibitors. Their properties, along with previous data on isozyme properties, allowed us to develop a new protocol for their selective measurement in crude extracts of various tissues and cell lines.

EXPERIMENTAL PROCEDURES

Chemicals and Reagents. Ni^{2+}-nitriloacetic acid superflow resin (NiNTA) was purchased from Qiagen. TALON metal affinity resin was from Clontech. All reagents and solvents used for the chemical synthesis of multisubstrate inhibitors below reported were purchased from Aldrich Chemical Co. Silica gel 60 F_{254} and RP-18 plates for thin layer chromatography (TLC) were from Merck. Tiazofurin riboside 5′-monophosphate (TrMP[1]) and tiazofurin adenine dinucleotide (TAD^+) were kindly provided by Prof. M. Grifantini (University of Camerino). Other biochemicals, unless otherwise indicated, were from Sigma.

Tissue Collection, Cell Line Culturing, and Crude Extract Preparation. Human liver and brain tissues from surgery were obtained from a local hospital and stored at −80 °C after immediate freezing in liquid nitrogen. Each sample was thawed on ice, cut in small pieces, and disrupted in a glass-Teflon Potter homogenizer in 20 mM Tris-HCl buffer (pH 7.5), 0.15 M NaCl, 1% Nonidet P40, 5 mM EDTA, 1 mM DTT, 1 mM PMSF, 0.02 mg/mL leupeptine, antipain, chymostatin, pepstatin, and aprotinin (5 mL/g of tissues). After clarification by centrifugation (16000*g*, 10 min at 4 °C), the crude protein extracts were dialyzed against 20 mM HEPES−KOH (pH 7.5), 1 mM DTT. Human hepatocellular carcinoma cell lines, SK-HEP1 and HepG2, were purchased from American Type Culture Collection (ATCC, Baltimore, MD). Human neuroblastoma SH-SY5Y cell line was provided by Prof. S. Amoroso (University of Ancona, Italy). Cell lines were subcultured as reported in the ATCC website (www.atcc.org), and, after cell disruption by passage through a 20-gauge needle, protein extracts were obtained as described above.

Cloning and Expression of the Three Human NMNAT Isozymes. NMNAT2 cDNA, cloned in the pET15b vector, was expressed in *Escherichia coli* BL21(DE3) following induction with 1 mM IPTG for 2 h (*27*). NMNAT1 (840 bp) and NMNAT3 (759 bp) open reading frames were amplified by RT-PCR (*28*) from total RNA isolated from the human adenocarcinoma cell line MCF7 (ATCC). Appropriate primers carrying restriction overhangs for directional cloning into the polylinker region of the pTrcHisA vector (Invitrogen) were used, i.e., AT1-fw and AT1-rev for NMNAT1, and AT3-fw and AT3-rev for NMNAT3 (see Supporting Information, Table 1). Directional cloning was performed at *Bam*HI/*Hin*dIII sites for NMNAT1 or at *Xho*I/*Eco*RI sites for NMNAT3. The resulting constructs, pTrcHisA-NMNAT1 and pTrcHisA-NMNAT3, were replicated in *E. coli* TOP10F′ (Invitrogen) and verified by sequencing before use in protein expression in the same bacterial strain. Cultures were grown to a final $OD_{600nm} \approx 0.6$ in an incubator shaker (200 rpm) at 37 °C in Luria−Bertani medium, supplemented with 100 μg/mL ampicillin, at which point induction was initiated by adding 1 mM IPTG followed by incubation for 12−14 h.

Purification of Human NMNAT Isozymes. All steps were performed at 4 °C. Induced cells, carrying pET15b-NMNAT2 (*27*) or the two above pTrcHisA plasmids encoding for NMNAT1 and NMNAT3, were harvested by centrifugation (5000*g*, 10 min), resuspended in 1/20 vol of original culture, and lysed by French Press (18 000 psi) in the following lysis buffers: 50 mM Na-phosphate (pH 8.0), 300 mM NaCl, 10 mM imidazole (for NMNAT1 and NMNAT3), or 50 mM Na-phosphate (pH 7.5), 500 mM NaCl, 1 mM $MgCl_2$, 5 mM CHAPSO (for NMNAT2), freshly supplemented with 1 mM PMSF, 1 mM TCEP, and 0.02 mg/mL leupeptine, antipain, chymostatin, pepstatin, and aprotinin. These crude extracts were clarified by centrifugation at 27000*g* for 20 min for subsequent purification. The His-tagged NMNAT1 and NMNAT3 proteins were purified by NiNTA affinity chromatography. Briefly, the clarified supernatants were loaded onto NiNTA columns (0.2 mL of resin per mL of crude extract) previously equilibrated with 50 mM Na-phosphate (pH 8.0), 300 mM NaCl, 1 mM TCEP, 10 mM imidazole. After washing each column with 50 mM imidazole in the same buffer and discarding the flow-through, the elution of both recombinant proteins was carried out by a linear increase of imidazole concentration up to 150 mM. The His-tagged NMNAT2 protein was purified by TALON affinity chro-

[1] Abbreviations: Ap_4A, P^1,P^4-di(adenosine-5′)-tetraphosphate; Ap_5A, P^1,P^5-di(adenosine-5′)-pentaphosphate; CHAPSO, 3-[(3-cholamidopropyl)dimethylammonio]-2-hydroxy-1-propanesulfonate; DTT, dithiothreitol; HEPES, 2-[4-(2-hydroxyethyl)-1-piperazinyl]ethanesulfonic acid; IPTG, isopropyl-β-D-thiogalactopyranoside; NHD^+, nicotinamide hypoxanthine dinucleotide; NGD^+, nicotinamide guanine dinucleotide; Np_3AD, P^1-(nicotinamide-riboside-5′)-P^3-(adenosine-5′)-triphosphate; Np_4AD, P^1-(nicotinamide-riboside-5′)-P^4-(adenosine-5′)-tetraphosphate; Nap_4AD, P^1-(nicotinate-riboside-5′)-P^4-(adenosine-5′)-tetraphosphate; PMSF, phenylmethylsulfonylfluoride; 3-carbamoyl-RPPI, 3-carbamoyl-1-β-D-ribofuranosylpyridinium hydroxide-5′-phosphoimidazolide; 3-carboxyl-RPPI, 3-carboxyl-1-β-D-ribofuranosylpyridinium hydroxide-5′-phosphoimidazolide; RT-PCR, reverse transcription-polymerase chain reaction; TAD^+, tiazofurin adenine dinucleotide; TCEP, tris-(2-carboxyethyl)phosphine; TMS, tetramethylsilane; TrMP, tiazofurin riboside 5′-monophosphate.

matography as follows. The clarified *E. coli* extract was loaded onto a TALON column (0.2 mL of resin per mL of crude extract) previously equilibrated with lysis buffer. After washing the resin with 50 mM Na-phosphate (pH 7.0), 500 mM NaCl, 1 mM $MgCl_2$, 20 mM imidazole, the recombinant protein was eluted with a linear gradient from 20 to 200 mM imidazole in the same buffer. Chromatographic fractions were subjected to SDS−PAGE (*29*) and assayed for NMNAT by a coupled assay (*30*). Active and homogeneous fractions were pooled and stored at 4 °C. Protein concentration was determined by the Bradford method (*31*), using BSA as the standard.

Chemical Synthesis and Characterization of Multisubstrate Inhibitors. The polyphosphate NAD^+ analogues Np_3AD and Np_4AD, as well as the deamido nicotinic derivative Nap_4AD, consisting of adenosine monophosphate and nicotinamide or nicotinate mononucleotide linked by a linear (5′- to 5′-) mono- or diphosphate bridge, were synthesized as follows. The chemical procedure started from the synthesis of 3-carbamoyl-RPPI. A solution of commercial NMN (0.076 mmol) was coevaporated with dry *N*,*N*-dimethylformamide (DMF) (2 × 2 mL) and then dissolved in DMF (3 mL). To the resulting solution 1,1′-carbonyldiimidazole (CDI) (0.76 mmol) was added, and the mixture was stirred at room temperature for 4 h; the reaction was monitored by ^{31}P NMR (D_2O: s −10.4 ppm). The excess of CDI was destroyed by addition of dry MeOH (67 μL) stirring for 30 min. Similarly, a deamidated version of the above compound, namely, the 3-carboxyl-RPPI, was prepared starting from the commercial NaMN (0.12 mmol). The resulting amidated and deamidated compounds were obtained in quantitative yield and used directly, without further purification, for the coupling reactions as follows.

Nuclear magnetic resonance spectra were recorded on a Varian-Mercury Plus AS400 spectrometer using tetramethylsilane (TMS) and H_3PO_4 as internal standards for ^1H NMR and ^{31}P NMR, respectively. Chemical shifts are reported in parts per million (δ) as s (singlet), d (doublet), t (triplet), q (quartet), m (multiplet), or br s (broad singlet). Mass spectroscopy was carried out on an HP 1100 MSD G19/46A instrument. All measurements were performed in a negative ion mode using atmospheric pressure electrospray ionization (API-ESI).

The Np_3AD synthesis was initiated by adding 3-carbamoyl-RPPI (0.06 mmol) with stirring to a dry DMF solution containing 0.066 mmol ADP (as tri-(*n*-butyl)ammonium salt, obtained by treatment of the corresponding free acid with tri-(*n*-butyl)amine in methanol). After stirring at 28 °C for 3 days, the ^{31}P NMR (D_2O) analysis showed the disappearance of the imidazolide. The reaction mixture was concentrated *in vacuo*, and the residue was dissolved in H_2O (10 mL) and then extracted with $CHCl_3$ (2 × 10 mL). The concentrated aqueous layer was applied to a DEAE-Sephadex column (HCO_3^- form) and eluted with a linear gradient of 0−0.6 M triethyl ammonium bicarbonate buffer (TEAB). The appropriate fraction containing Np_3AD was evaporated to dryness and dried by coevaporations with dry ethanol to give the compound as triethyl ammonium salt as a white solid (20% yield). ^1H NMR (D_2O, 400 MHz): δ 4.25 (m, 2H, H-5′a, H-5′b Ado), 4.38 (m, 2H, H-5′a, H-5′b N), 4.52 (m, 4H, H-3′, H-4′Ado, and H-3′, H-4′ N), 4.70 (m, 2H, H-2′ Ado, and H-2′ N), 6.08 (d, J = 6.1 Hz, 1H, H-1′ Ado), 6.15 (d, J = 5.5 Hz, 1H, H-1′ N), 8.28 (m, 1H, H-5 N), 8.33 (s, 1H, H-2 Ado), 8.55 (s, 1H, H-8 Ado), 8.90 (d, J = 8.1 Hz, 1H, H-4 N), 9.27 (d, J = 6.2 Hz, 1H, H-6 N), 9.38 (s, 1H, H-2 N). ^{31}P NMR (D_2O, 162 MHz): δ −11.0 (br s, 2P, CH_2OP−), −22.6 (m, 1P, O−P−O). MS: *m*/*z* 743.4 $[M - H]^-$.

The Np_4AD synthesis was initiated by adding 3-carbamoyl-RPPI (0.06 mmol) with stirring to a dry DMF solution containing 0.066 mmol of ATP (tri-(*n*-butyl)ammonium salt), as above described for Np_3AD. Np_4AD was obtained as triethyl ammonium salt as a white solid (21% yield). ^1H NMR (D_2O, 400 MHz): δ 4.12 (m, 2H, H-5′a, H-5′b Ado), 4.23 (m, 2H, H-5′a, H-5′b N), 4.41 (m, 4H, H-3′, H-4′ Ado, and H-3′, H-4′ N), 4.63 (m, 2H, H-2′Ado, and H-2′ N), 5.90 (d, J = 6.4 Hz, 1H, H-1′ Ado), 5.97 (d, J = 5.5 Hz, 1H, H-1′ N), 8.08 (s, 1H, H-2 Ado), 8.12 (m, 1H, H-5 N), 8.32 (s, 1H, H-8 Ado), 8.73 (d, J = 8.1 Hz, 1H, H-4 N), 9.12 (d, J = 5.8 Hz, 1H, H-6 N), 9.22 (s, 1H, H-2 N). ^{31}P NMR (D_2O, 162 MHz): δ −11.4, −11.8 (2dd, 2P, CH_2OP−), −23.4 (dd, 2P, O−P−O). MS: *m*/*z* 823.3 $[M - H]^-$. A very partial version of the procedure for the synthesis of the above amidated dinucleoside polyphosphates has been published in a preliminary report (*32*).

Synthesis of the corresponding nicotinate analogue, Nap_4AD, was initiated by adding 3-carboxyl-RPPI (0.15 mmol) with stirring to a dry DMF solution containing 0.16 mmol of ATP (tri-(*n*-butyl)ammonium salt), as described above. Nap_4AD was obtained as triethyl ammonium salt as a white solid (25% yield). ^1H NMR (400 MHz, D_2O): δ 4.10 (m, 2H, H-5′a, H-5′b Ado), 4.25 (m, 2H, H-5′a, H-5′b N), 4.36 (m, 3H, H-2′, H-3′, H-4′ Ado), 4.62 (m, 3H, H-2′, H-3′, H-4′ N), 5.93 (2d overlapped, 2H, H-1′ Ado, and H-1′ N), 8.05 (m, 1H, H-5 N), 8.10 (s, 1H, H-2 Ado), 8.33 (s, 1H, H-8 Ado), 8.70 (d, J = 8.1 Hz, 1H, H-6 N), 9.02 (s, 1H, H-2 N), 9.08 (d, J = 6.4 Hz, 1H, H-4 N). ^{31}P NMR (D_2O, 162 MHz): δ −10.45, −10.76 (2dd, 2P, CH_2−OP−), −22.30 (dd, 2P, O−P−O). MS: *m*/*z* 825.3 $[M - H]^-$.

NMN Adenylyltransferase Activity Assays. NMNAT activity was measured by a HPLC-based assay (*30*), with the following modifications: (a) the HPLC column was thermostated at 25−30 °C to improve the separation efficiency; (b) when NADH formation was assayed, the reaction was stopped by boiling to prevent NADH degradation. The standard reaction mixture contained 27 mM HEPES−KOH (pH 7.5), 20 mM $MgCl_2$, 1 mM DTT, 0.5 mg/mL BSA, 1 mM of both NMN and ATP substrates, and 0.002−20 μg/mL purified recombinant protein. Crude extracts from tissues or cell lines were assayed using 20−60 μg/mL of protein in standard mixtures supplemented with 10 mM NaF. Reaction was performed at 37 °C. The above conditions were used for measuring the optimal NMNAT activity.

Metal ion effects were assayed by replacing $MgCl_2$ in the standard mixture with 0−25 mM each of the following salts: $CaCl_2$, $FeCl_3$, $NiCl_2$, $CoCl_2$, $CrCl_3$, $MnCl_2$, and $ZnCl_2$. For these experiments, the enzyme preparations were previously dialyzed against 20 mM HEPES−KOH (pH 7.5), 1 mM DTT.

The individual contribution to NAD^+ formation by each of the three NMNAT isozymes was selectively evaluated in a reaction mixture composed of 27 mM HEPES−KOH buffer (pH 7.5), 10 mM NaF, 1 mM DTT, 1 mM NMN, supplemented with 2 mM $ZnCl_2$ and 1 mM ATP for

NMNAT1, 20 μM $MgCl_2$ and 1 mM ATP for NMNAT2, 20 mM $MgCl_2$ and 1 mM ITP for NMNAT3. Individual activities were calculated from NAD^+ formation (NMNAT1 and NMNAT2) and NHD^+ formation (NMNAT3) and normalized to the optimal activity by multiplying for the following factors: 1.053 for NMNAT1, 3.846 for NMNAT2, and 6.41 for NMNAT3.

Statistical Analysis of Rate Data. All reaction rates were obtained as tangent lines in the linear region of plots of product formation *versus* time, using multiple time points. All rates were measured in triplicate, and the reported data are averaged values with standard errors within acceptable confidence limits in all cases (see Tables 1 to 4). One unit (U) of activity is defined as the amount of enzyme needed to catalyze the synthesis of 1 μmol of product per minute under standard assay conditions. As further evidence that the velocities were obtained for the initial-rate phase, all rate data were analyzed by nonlinear least-squares regression using the KaleidaGraph software (Synergy Software, Inc., Reading, Pennsylvania) for plots of v *versus* [NMN] or v *versus* [ATP]. A sample plot is provided in the Supporting Information. With one substrate held at a constant but nonsaturating concentration, the initial velocities were fitted to the equation $v = V_{m,app}[S]/([S] + K_{m,app})$, where $V_{m,app}$ is the apparent maximal velocity, [S] is the substrate concentration, and $K_{m,app}$ is the apparent Michaelis−Menten constant. In all cases, the regression lines fit the data with R values of 0.985 or above, and all reported rate parameters were likewise obtained by regression analysis. These parameters also allowed us to construct plots of $1/v$ *versus* 1/[NMN] or $1/v$ *versus* 1/[ATP] showing the original experimental rate data but with theoretical lines based on slopes and intercepts that were calculated from best-fit apparent values of $V_{m,app}$ and $K_{m,app}$.

The kinetic mechanism of the NMNAT-catalyzed reaction was established by evaluating the inhibition pattern exerted on reaction velocity in the forward direction, by either of the products PP_i, NAD^+ (as well as the alternative product $NaAD^+$) or by the multisubstrate inhibitors Np_3AD, Np_4AD, and Nap_4AD (*33*, *34*). The inhibition rate data were fitted to the generalized rate equation for readily reversible inhibitors, $v = V_{max}[S]/[K_m(1 + I/K_i) + [S](1 + I/\alpha K_i)]$, where the parameter α provides a quantitative measure of the inhibition mechanism according to ref *35*. In particular, the value of α indicates whether the observed inhibition is competitive ($\alpha = \infty$), purely noncompetitive ($\alpha = 1$), or of a mixed-type ($\alpha < 1$ or $\alpha > 1$). We likewise constructed plots of $1/v$ *versus* 1/[S] with the original experimental rate data and theory lines having slopes and intercepts based on the best-fit rate parameters from the regression analysis of inhibition data.

Formation of nonproductive abortive complexes in the presence of product inhibitors is known to alter the kinetic behavior of multisubstrate enzyme reactions and is manifested as concave upward $1/v$ versus 1/[S] plots at high concentrations of the varied substrate (*36*). We should stress, however, that the observed patterns for our NMNAT product inhibition data showed little or no indication of abortive complex formation, as evidenced by the distinctly linear regions of $1/v$ *versus* 1/[NMN] or $1/v$ *versus* 1/[ATP] in the absence and presence of several fixed concentrations of product.

Table 1: Kinetic Parameters of Human NMNAT Isozymes

substrate:	ATP[a]			NMN[a]			NaMN[b]			NMNH[b]		
	K_m (μM)	k_{cat} (s^{-1})	k_{cat}/K_m ($s^{-1}\,M^{-1}$)	K_m (μM)	k_{cat} (s^{-1})	k_{cat}/K_m ($s^{-1}\,M^{-1}$)	K_m (μM)	k_{cat} (s^{-1})	k_{cat}/K_m ($s^{-1}\,M^{-1}$)	K_m (μM)	k_{cat} (s^{-1})	k_{cat}/K_m ($s^{-1}\,M^{-1}$)
NMNAT1	58.5 ± 4.2	53.9 ± 1.4	9.20×10^5	22.3 ± 2.6	53.8 ± 3.4	24.1×10^5	67.7 ± 2.2	42.9 ± 0.5	6.33×10^5	294 ± 27	18.6 ± 0.7	0.63×10^5
NMNAT2	88.9 ± 18.3	8.8 ± 0.4	0.99×10^5	21.3 ± 2.7	8.8 ± 0.3	4.11×10^5	14.5 ± 2.6[c]	6.9 ± 0.1	4.79×10^5	304 ± 36	3.3 ± 0.3	0.11×10^5
NMNAT3	42.1 ± 5.8	2.5 ± 0.3	0.58×10^5	66.2 ± 8.5	2.5 ± 0.2	0.38×10^5	111 ± 21	3.8 ± 0.2	0.34×10^5	130 ± 12	7.2 ± 0.6	0.55×10^5

[a] Kinetic parameters were calculated using both fixed and variable substrate concentrations in the range 12.5−500 μM. [b] Apparent kinetic parameters were calculated by varying NaMN and NMNH concentrations from 40 μM to 1 mM in the presence of 1 mM ATP. [c] Should be considered as an estimate since the lowest variable substrate concentration used was 40 μM.

Table 2: Product Inhibition Behavior of Human NMNAT Isozymes

product:[a]	PPi				$NaAD^+$				NAD^+			
substrate:[b]	NMN		ATP		NMN		ATP		NaMN		ATP	
	K_i (μM)	inhibn type[c]	K_i (μM)	inhibn type[c]	K_i (μM)	inhibn type[c]	K_i (μM)	inhibn type[c]	K_i (μM)	inhibn type[c]	K_i (μM)	inhibn type[c]
NMNAT1	390.4 ± 41.7	NC	175.3 ± 34.9	NC	502.5 ± 44.1	M	305.5 ± 9.4	C	418.3 ± 13.5	M	749.0 ± 29.6	C
NMNAT2	160.7 ± 16.4	M	361.2 ± 39.4	M	41.0 ± 1.1	M	23.0 ± 0.7	C	67.2 ± 10.4	M	95.9 ± 2.3	C
NMNAT3	1155.5 ± 93.0	M	334.0 ± 23.5	M	364.7 ± 33.7	C	205.1 ± 15.8	M	1017.4 ± 186.0	C	1418.0 ± 195.0	M

[a] Assayed at concentrations of 0, 0.2, 0.5, and 1 mM. [b] Fixed substrate was 3-fold the K_m, while variable substrate was ranged between half and twice the K_m (see the K_m values in Table 1). [c] Deduced according to ref *35* and referred to as "competitive" (C), "noncompetitive" (NC), or "mixed" (M).

Real-Time Quantitative RT-PCR. Real-time PCR experiments were performed on a Rotor-Gene 3000 equipment (Corbett Research, Hilly St. Mortlake, NSW 2137, Australia), using SYBR green detection. DNAse-treated total RNA samples were extracted from SK-HEP1, HepG2, and SH-SY5Y cell lines ($2-5 \times 10^6$ cells) using a SV Total RNA Isolation kit (Promega). RNA yield and quality were estimated spectrophotometrically and electrophoretically (*28*). First-strand cDNA was synthesized using M-MuLV reverse transcriptase and random nonamer primers (First-Strand cDNA Synthesis Kit, Bio Basic, Inc.). Control mixtures lacking reverse transcriptase were prepared in parallel to estimate the genomic DNA contamination. The real-time PCR reaction mixtures (25 μL final volume) contained 200 ng of transcribed total RNA as template, 10 mM Tris-HCl buffer (pH 8.3), 50 mM KCl, 200 μM dNTPs, 3 mM $MgCl_2$, 1.25 U of JumpStartTM Taq DNA polymerase, 1:20000 (v/v) SYBR Green I (Molecular Probes, Inc., USA), and 250 nM of each primer pair, namely, RT1-fw and RT1-rev for NMNAT1, RT2-fw and RT2-rev for NMNAT2, and RT3-fw and RT3-rev for NMNAT3 (see Supporting Information, Table 1). The housekeeping 18S rRNA signal was amplified by using the same mixture in the presence of 4 mM $MgCl_2$ and 400 nM of both RNA18S-fw and RNA18S-rev primers. PCR cycling was 94 °C for 1 min, followed by 45 cycles of 94 °C for 20 s, 58 °C for 20 s, and 72 °C for 20 s for fluorescence acquisition. A relative quantification of individual signals toward the housekeeping was performed using the $2^{-\Delta\Delta Ct}$ method (*37*). Under the above optimized PCR conditions, the efficiency and specificity of the reaction were maximal for all signals analyzed. Genomic DNA contamination in all extracted RNA samples was insignificant (<5%).

RESULTS

Initial-Rate Kinetics of Human NMN Adenylyltransferase Isoenzymes. In our kinetic studies on the human NMN adenylyltransferases, we used recombinant enzyme isoforms that were bacterially expressed with a hexa-histidine tag to facilitate their one-step purification by metal affinity chromatography (Supporting Information, Table 2). The final enzyme preparations were homogeneous by SDS−PAGE, with expected molecular masses of 36 kDa for NMNAT1, 37 kDa for NMNAT2, and 32.7 kDa for NMNAT3 (Supporting Information, Figure 1). Notably, all three His-tagged NMNATs were as active and had the same pH and temperature optima as wild-type enzymes lacking the hexa-histidine tag (*26*).

Because the kinetic mechanism was only known for NMNAT isozyme 1, we conducted corresponding initial-rate experiments to determine the patterns of $1/v$ *versus* 1/[ATP] at various constant concentrations of the cosubstrate NMN, and $1/v$ *versus* 1/[NMN] (or $1/v$ *versus* 1/[NaMN]) at various constant concentrations of ATP. All rate data gave patterns where the lines intersected to the left of the $1/v$ axes (not shown), and were thus consistent with the sequential ternary complex kinetic mechanisms. The corresponding rate parameters (K_m, k_{cat}, and k_{cat}/K_m), derived from a nonlinear curve fitting on the primary plot (see Supporting Information, Figure 2), are listed in Table 1. The catalytic efficiency with respect to the above substrates, calculated as the ratio between k_{cat} (turnover number) and K_m, indicated (a) a higher efficiency of NMNAT1 with respect to the other two isozymes, NMNAT3 being the least catalytically efficient; (b) a preference of NMNAT1 in the utilization of NMN compared to NaMN. In contrast, no such substrate preference has been found for NMNAT2 and NMNAT3. Table 1 also shows that all three enzymes are able to utilize NMNH as a substrate. This was not unexpected in that, since the first characterization of a homogeneous enzyme preparation, we observed that NMNAT was competitively inhibited by NMNH, suggesting that it could also act as a substrate (*38*). Indeed, we found that human and bovine enzymes catalyze the synthesis of NADH (*10*, *26*, *39*). These results suggest a potential role of NMNAT in regulating the redox state of the cell, i.e., the ratio NAD^+/NADH. Also, the direct synthesis of NADH could play an important role in mitochondria. Indeed, by inspecting the catalytic efficiencies reported in Table 1, it could be observed that the mitochondrial NMNAT3, the least catalytically efficient, shows a k_{cat}/K_m value for NADH formation significantly higher than NMNAT2 and similar to that exhibited by NMNAT1.

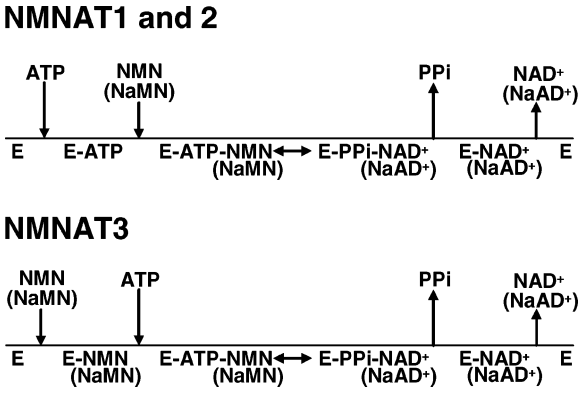

FIGURE 1: Steady-state kinetic mechanisms of the three human NMNAT isozymes. The schemes, according to Cleland's nomenclature (*33*), were inferred from the inhibition patterns illustrated in Table 2.

Table 3: Multisubstrate Geometric Analogue Inhibition of Human NMNAT Isozymes

	K_i (μM)							
inhibitor:[a]	Np_3AD		Np_4AD		Nap_4AD		Nap_4AD	
substrate:[b]	NMN	ATP	NMN	ATP	NMN	ATP	NaMN	ATP
NMNAT1	89.0 ± 2.1	56.3 ± 1.8	31.1 ± 3.0	49.2 ± 5.4	67.9 ± 9.2	59.1 ± 5.6	36.9 ± 0.3	84.5 ± 6.8
NMNAT2	31.5 ± 6.4	35.9 ± 6.5	25.8 ± 3.2	24.2 ± 3.2	328.3 ± 67.9	174.5 ± 16.5	125.7 ± 17.4	657.6 ± 73.4
NMNAT3	66.8 ± 1.7	40.6 ± 1.1	73.6 ± 5.9	29.8 ± 3.9	88.3 ± 9.3	32.8 ± 3.9	21.7 ± 0.7	43.1 ± 0.7

[a] Assayed at concentrations of 0, 30, and 70 μM. [b] Fixed substrate was 3-fold the K_m, while variable substrate was ranged between half and twice the K_m (see the K_m values in Table 1).

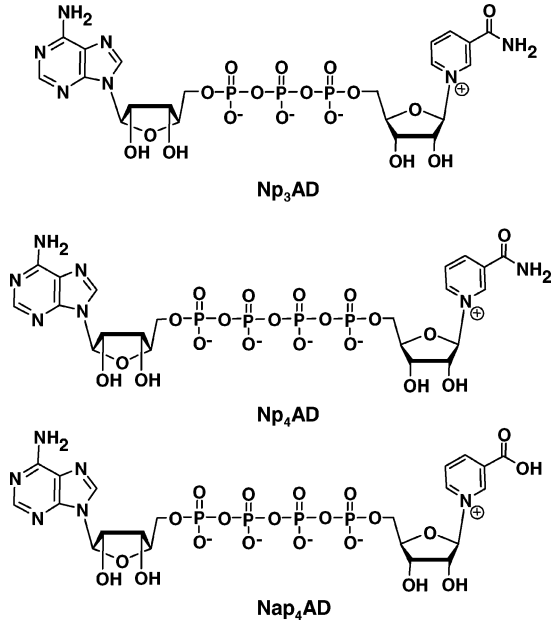

FIGURE 2: P^1-(nicotinamide/nicotinate-riboside-5′)-P^n-(adenosine-5′) dinucleotides used as multisubstrate geometric inhibitors. In the chemical mechanism for adenylyl group transfer to NMN, nucleophilic attack occurs on the α-phosphoryl of ATP, with expulsion of the pyrophosphate leaving group. By analogy to the phosphoryl transfer reactions of adenylate kinase, which is inhibited by the naturally occurring Ap_4A and synthetic Ap_5A, we hypothesized that NMNAT maybe inhibited by the corresponding dinucleotides Np_3AD, Np_4AD, and Nap_4AD, the structures of which are shown here.

The order of substrate addition for NMNAT2 and NMNAT3 was inferred from product inhibition experiments. Pyrophosphate was used as the common product in measurements of the rate of NAD^+ and $NaAD^+$ formation. $NaAD^+$ was used as an alternative product in NAD^+ synthesis; likewise, NAD^+ was used as an alternative product in $NaAD^+$ synthesis. This approach allowed us to use HPLC to measure the formation of the specific dinucleotide formed by the enzyme in the presence of the inhibiting dinucleotide. The inhibition patterns shown in Table 2 allowed us to tentatively assign the kinetic mechanism shown in Figure 1, where ATP binds first in the case of NMNAT1 and NMNAT2, but NMN is the first substrate to bind to NMNAT3. Previous kinetic studies (*34*, *38*) on NMN adenylyltransferase isozyme 1 isolated directly from human tissues were consistent with ordered Bi-Bi mechanism, using Cleland's nomenclature (*33*). In all cases, the products are released sequentially, with PP_i first, followed by NAD^+. All rate parameters for these inhibition studies are also presented in Table 2.

Multisubstrate Geometric Inhibitors. With the exception of gallotannin, a polyphenolic plant metabolite that inhibits all three human NMNATs (*25*) as well as other enzymatic activities (*40*−*42*), all previous efforts to identify effective NMNAT inhibitors for kinetic and metabolic studies were fruitless (*23*, *26*). Recognizing the potential utility of enzyme inhibitors for mechanistic studies and for use as enzyme-specific metabolic inhibitors, we decided to synthesize and test multisubstrate geometric inhibitors analogous to the adenylate kinase inhibitors P^1,P^4-di(adenosine-5′)-tetraphosphate (Ap_4A) and P^1,P^5-di(adenosine-5′)-pentaphosphate (Ap_5A) (*43*, *44*). Such inhibitors offer the advantage that they can simultaneously occupy both substrate subsites within the active sites of enzymes displaying sequential ternary complex kinetic mechanisms (*36*). Because NMNAT catalyzes its reaction via ternary complex formation (Figure 1), the enzyme should be effectively and specifically inhibited by multisubstrate analogues possessing the features of NMN and AMP, but connected by additional phosphoryl-unit linkers.

Based on this rationale, we developed a two-step synthetic method for obtaining the three novel asymmetric dinucleotides: P^1-(adenosine-5′)-P^3-(nicotinamide-riboside-5′)-triphosphate (Np_3AD), P^1-(adenosine-5′)-P^4-(nicotinamide-riboside-5′)-tetraphosphate (Np_4AD), and P^1-(adenosine-5′)-P^4-(nicotinic-acid-riboside-5′)-tetraphosphate (Nap_4AD) (Figure 2). We used 1,1′-carbonyldiimidazole to form the corresponding phosphoimidazolides of NMN or NaMN, followed by condensation with tri-(*n*-butyl)ammonium salts of ADP or ATP in dry DMF. Condensation reaction conditions were optimized by monitoring the disappearance of the imidazolide by ^{31}P NMR (in D_2O). These novel dinucleotides were then purified and characterized by NMR and mass spectroscopy, as described under Experimental Procedures.

Table 3 lists the inhibition constants for these multisubstrate geometric inhibitors for all three human NMNATs. These agents inhibit the three isozymes at sub-millimolar range, and their inhibition patterns (data not shown) with respect to the individual substrates were also consistent with the ordered kinetic mechanisms indicated in Figure 1. We observed that Np_3AD and Np_4AD were more effective inhibitors of isozyme 2, whereas Nap_4AD inhibits isozyme 1 and 3 more effectively than isozyme 2.

In principle, an enzyme's affinity for a multisubstrate geometric analogue should be determined by the sum of the individual binding energies of the individual substrates (i.e., $\Delta G_{Analogue} = \Delta G_{Substrate-A} + \Delta G_{Substrate-B}$), as reflected in the values of the analogue's inhibition constant $K_{Analogue}$ and the individual substrate dissociation constants K_{iS} (i.e., $K_{Analogue} = K_{iSubstrate-A} \times K_{iSubstrate-B}$). Even though Np_3AD, Np_4AD, and Nap_4AD were experimentally found to be considerably less potent than predicted by these relationships, these dinucleoside polyphosphates are still the most effective NMNAT inhibitors characterized to date.

Table 4: Properties of TrMP[a] as an Alternative Substrate of Human NMNAT Isozymes

isozyme	K_m (mM)	k_{cat} (s^{-1})	k_{cat}/K_m (s^{-1} mM^{-1})
NMNAT1	0.37 ± 0.04	14.9 ± 0.74	40.27
NMNAT2	>100	0.55	<0.0055
NMNAT3	2.01 ± 0.50	0.42 ± 0.08	0.209

[a] Tiazofurin riboside 5′-monophosphate was assayed at 0.05, 0.1, 0.2, 0.4 and 1 mM in the presence of 1 mM ATP.

Action of Human NMNAT Isozymes on Alternative Nucleoside 5′-Triphosphate Substrates. An earlier study of the archaeal *Methanococcus jannaschii* NMNAT enzyme revealed an unexpected flexibility with respect to utilization of GTP and ITP in the synthesis of NGD^+ and NHD^+, respectively (*45*, *46*). By comparing the three-dimensional crystal structures of human NMNATs with the *M. jannaschii* enzyme, we observed a striking similarity between the active sites of human isozyme 3 and the archaeal enzyme (G. Magni, unpublished). This structural similarity probably explains the ability of human isozyme 3 to synthesize NGD^+ and NHD^+ (*25*), and we have obtained the following kinetic constants: for GTP, $K_m = 276 \pm 79$ μM and $k_{cat} = 0.34 \pm 0.04$ s^{-1}, and for ITP, $K_m = 350 \pm 53$ μM and $k_{cat} = 0.72 \pm 0.04$ s^{-1}. By contrast, isozymes 1 and 2 were almost inactive in NHD^+ synthesis, and likewise produced very low amounts of NGD^+ (*14*, *46*). Interestingly, NHD^+ was found in mitochondria more than three decades ago (*47*), even though the enzymatic basis for its synthesis was then unknown.

As noted earlier, tiazofurin monophosphate (TrMP) is converted by NMNAT into tiazofurin adenine dinucleotide (TAD^+), and this metabolic transformation is thought to underlie the antineoplastic action of the prodrug tiazofurin (*15*−*17*). Because each NMNAT isozyme has its own unique subcellular location, identification of the isozyme(s) that can convert TrMP to TAD^+ may provide important clues about the target organelle for this important antineoplastic agent. These considerations led us to consider the possibility that certain human NMNAT isozymes may be more efficient. Significantly, we found that NMNAT1 and NMNAT3 were both capable of synthesizing TAD^+ from TrMP, albeit at significantly different rates, (Table 4). In contrast, repeated assays revealed that TAD^+ formation by NMNAT2 is inconsequentially slow. Thus, it might be concluded that NMNAT2 isozyme does not represent the physiological target for chemotherapeutic strategies based on tiazofurin administration.

The mitochondrial location of NMNAT3 reinforces the possibility that NAD^+ analogues could in fact be formed in this organelle, but their physiological relevance as coenzymes *in vivo* has never been established.

Utility of Substrate and Metal Ion Selectivity to Discriminate NMNAT Isozymes. To date, there is no information on the relative contribution of NMNAT isozymes to NAD^+ formation. We recognized, however, that these isozymes might be discriminated in experiments based on their distinctive substrate utlization, and metal ion and inhibitor effects.

NMNAT activity requires the presence of divalent cations (*26*), and we therefore decided to determine whether the metal ion requirement could be used as a method to discriminate isozymes 1, 2, and 3. We therefore evaluated the activity of NMNAT isozymes in the presence of various

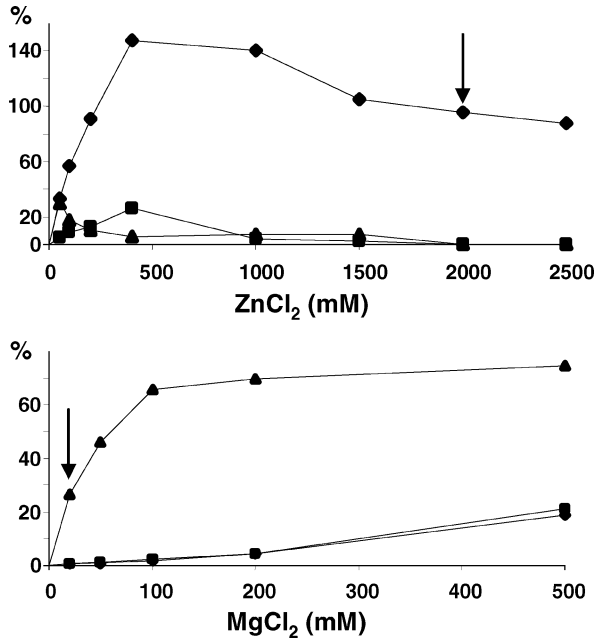

FIGURE 3: Selective discrimination of NMNAT isozyme activity by metal ions. Recombinant NMNAT1 (◆), NMNAT2 (▲), and NMNAT3 (■) were assayed at various concentrations of Zn^{2+} or Mg^{2+} ions. Activities are referred to as the percentage of the activity measured with 20 mM $MgCl_2$ (optimal activity). Arrows indicate the ion concentration selected for discriminating NMNAT1 (top) and NMNAT2 (bottom) activities *in vitro*.

concentrations of the chloride salts of Ca^{2+}, Co^{2+}, Cr^{3+}, Fe^{3+}, Mg^{2+}, Mn^{2+}, Ni^{2+}, and Zn^{2+}. Of these, Mg^{2+} is the most effective ion with NMNAT2 and NMNAT3, whereas NMNAT1 prefers Zn^{2+}. The Zn^{2+} effect is important in that it distinguishes isozyme 1 from isozymes 2 and 3, which show activities in the presence of Zn^{2+} amounting to only 21% and 5.4% relative to isozyme 1.

We set about to establish normalization factors for comparing the activity of NMNAT isozymes under standardized assay conditions. Among the three isozymes, NMNAT3 is unique in terms of its use of ITP, albeit with a K_m that is some 10 times higher than that for ATP and with a V_{max} that is 30% of that for ATP. Therefore, at 1 mM ITP, the NMNAT3 activity was calculated to be 15.6% of that measured with 1 mM ATP. Based on the data in Figure 3, we concluded that (a) NMNAT1 activity can be selectively measured in the presence of 2 mM $ZnCl_2$, reaching 95% of the activity assayed with 20 mM $MgCl_2$; and (b) NMNAT2 activity can be discriminated by using 20 μM $MgCl_2$, a concentration sufficient to sustain 26% of the optimal activity. The above percentages have been used to calculate normalization factors of 1.053 for NMNAT1, 3.846 for NMNAT2, and 6.41 for NMNAT3, when assayed as defined under Experimental Procedures.

These discrimination factors were verified in assays where NMNAT1, NMNAT2, and NMNAT3 were combined in different proportions. Table 5 shows the results from a typical experiment, where no measurable interference among the mixed isozyme activities was observed. The same conclusion could be drawn also by mixing very different ratios of the three isozymes (not shown).

Discrimination of NMNAT Isoforms in Human Cell Extracts. We next wished to determine whether this approach was valid for discriminating the amounts of the various

Table 5: *In Vitro* Discrimination of Human NMNAT1, NMNAT2, and NMNAT3[a]

	activity (mU)			
	A	B	C	D
NMNAT1	0.139	0.129 (0.136)	nd[b]	nd
NMNAT2	0.812	nd	0.230 (0.885)	nd
NMNAT3	0.729	nd	nd	0.120 (0.774)
NMNAT(1+2+3)	1.578	0.127 (0.134)	0.225 (0.865)	0.104 (0.666)

[a] A typical experiment for the discrimination assay for the three recombinant human isozymes is presented. Extensively dialyzed NMNAT1, NMNAT2, and NMNAT3 preparations were assayed both separately and after their mixing as shown in the table. Assay conditions: (A) 27 mM HEPES-KOH buffer (pH 7.5), 10 mM NaF, 1 mM DTT, 1 mM NMN, 1 mM ATP, and 20 mM $MgCl_2$; (B) 20 mM $MgCl_2$ replaced by 2 mM $ZnCl_2$ (discriminating for NMNAT1); (C) 20 mM $MgCl_2$ replaced by 20 μM $MgCl_2$ (discriminating for NMNAT2); (D) 1 mM ATP replaced by 1 mM ITP (discriminating for NMNAT3). In parentheses, the normalized activity values are calculated as reported both in the text and in the Experimental Procedures. [b] Not detectable.

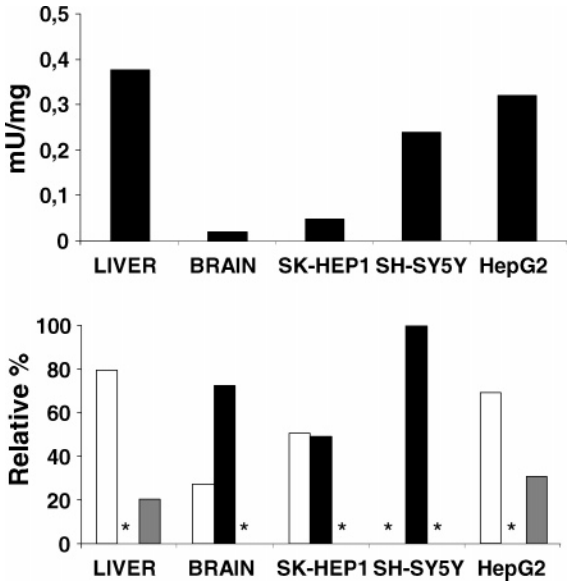

FIGURE 4: Determination of individual NMNAT isozymes in human tissues and cell lines. Top panel: NMNAT specific activity in dialyzed protein extracts from peritumoral human tissues (liver and brain), hepatocarcinoma (SK-HEP1 and HepG2), and neuroblastoma (SH-SY5Y) cell lines. The activity accounting for all isoenzymes was measured in the presence of 20 mM $MgCl_2$. Bottom panel: The relative percentage of NMNAT1 (white bars), NMNAT2 (black bars), and NMNAT3 (gray bars) in each of the above samples, as determined by the discrimination method. Data were normalized as described under Experimental Procedures. Asterisks indicate that no activity was detected under the described experimental conditions.

isozymes in cell extracts. Given the interest in NMNAT levels in healthy and cancerous cells, we worked with two peritumoral human tissues (i.e., normal liver and brain tissue obtained at the margin of excised tumor biopsy), as well as hepatocarcinoma cell lines SK-HEP1 and HepG2, and one neuroblastoma cell line SH-SY5Y. The dialyzed protein extracts were initially assayed using 20 mM $MgCl_2$ in order to evaluate the sum of all enzyme forms to observed activity. As shown in Figure 4 (top panel), different total NMNAT activity levels were observed, with higher activity observed in liver, SH-SY5Y, and HepG2 cells. Subsequent discrimination assays of the same extracts yielded the relative isozyme contributions, as diagrammed in the bottom panel of Figure 4. The result shows that, in all extracts, the three isozymes are not simultaneously present and do not contribute equally to NAD^+ formation. For example, in brain as well as neural SH-SY5Y cells, NMNAT3 is not detectable, whereas NMNAT2 predominates, in agreement with reported expression levels in neurons (*48*). In peritumoral liver tissue and in the two hepatic cell lines, however, the scenario is different: in addition to the expected predominance of NMNAT1 (*49*), NMNAT3 is only present in liver and HepG2 cells, while NMNAT2 was found exclusively in SK-HEP1 cells (Figure 4, bottom panel). The idea that the apparent replacement of NMNAT3 by NMNAT2 may be associated with malignancy is suggested by the fact that HepG2 cells, whose activity profile closely resembles that of normal (peritumoral) liver tissue, appears to be much less metastatic and invasive than SK-HEP1 cells (*50*).

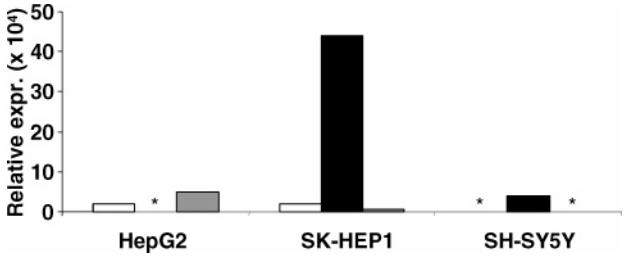

FIGURE 5: Real-time quantitative RT-PCR analysis of human cell lines. Relative expression of NMNAT1 (white bars), NMNAT2 (black bars), and NMNAT3 (gray bars) mRNAs with respect to the rRNA 18S housekeeping signal. Asterisks indicate that no isozyme-specific mRNA was detected under the described experimental conditions.

To validate our protocol, we measured isozyme-specific mRNA levels using reverse transcriptase to make the corresponding DNA sequences, followed by quantitative polymerase chain reaction (real-time PCR) on the above cell lines. Figure 5 shows the expression of the three NMNAT mRNAs, relative to the 18S rRNA housekeeping signal. This profile substantiates the activity profile reported in Figure 4b in that, in all three cell lines analyzed, the distinctive presence or absence of each isozyme perfectly matched. In particular, consistently with the activity detectable, no NMNAT2 mRNA was observed in HepG2 cells, where NMNAT3 mRNA appeared exclusively. The lack of NMNAT1 mRNA was also confirmed by the lack of NMNAT1 activity in SH-SY5Y cells. The lack of NMNAT1 protein in this cell line was also confirmed by Western blot analysis (not shown), performed with isozyme-1-targeted polyclonal antibodies (Igtech, Inc., Salerno, Italy), using the protein extract from the peritumoral liver tissue (where NMNAT1 is most abundant) as the positive control.

DISCUSSION

Because there are no known alternative pathways for NAD^+ biosynthesis, the enzyme NMN adenylyltransferase is indispensable for NAD^+ formation in most living organisms (*10*). The development of the multisubstrate geometric analogues Np_3AD, Np_4AD, and Nap_4AD for the human NMN adenylyltransferases, as described in this report, provides new tools for mechanistic as well as for metabolic studies on this important enzyme in NAD^+ biosynthesis. It is important to emphasize that these compounds are not transition-state analogues, because they do not mimic the

bond order and/or geometry of atoms at the reaction center in the activated transition-state complex. Therefore, these multisubstrate analogues would not be expected to exhibit the extraordinary binding energy of true transition-state analogues (*51*, *52*). Even so, based on the great practical utility of Ap_4A and Ap_5A in suppressing adenylate kinase activity (*43*, *44*), we believe that our NMNAT inhibitors will provide the opportunity to investigate important aspects of NAD^+ in many posttranslational modification reactions. Although Np_3AD, Np_4AD, and Nap_4AD are polyanions and hence cannot penetrate the peripheral membrane of target cells, these agents may be introduced into cells by microinjection, electroporation, or liposome carriers. Alternatively, one can use detergent-permeabilized cells to study the metabolic impact of these multisubstrate analogues. For such an approach to be feasible, it would be prudent to determine whether these agents inhibit other NAD^+-dependent processes.

Our finding of isozyme-specific differences in the kinetic mechanisms for substrate addition (Figure 1) deserves special mention, because it is not immediately clear what advantages are gained by an enzyme operating by means of an ordered sequential Bi-Bi pathway versus a random sequential Bi-Bi pathway. It should be stressed that the ordered ternary complex mechanism is a limiting case of a random mechanism, with one of the two pathways having become the dominant addition pathway. For example, creatine kinase is known to operate by a random ternary complex mechanism at pH 8 (*53*) and an ordered ternary complex kinetic mechanism at pH 7 (*54*). One potential clue is that each isozyme is organelle-specific, with NMNAT1 found in the nucleus, NMNAT2 in the Golgi apparatus, and NMNAT3 in the mitochondria. In this respect, the kinetic properties of each human NMNAT may have evolved to operate optimally within the unique microenvironment of its respective compartment. Because an ordered mechanism can be considered to be a limiting case of a random kinetic mechanism, and because binding of the leading substrate in an ordered pathway might improve the efficiency of second-substrate binding, we speculate that these enzymes may have adapted to optimize binding of a substrate that is less abundant in one or more of the subcellular compartments and/or to minimize the inhibitory effects of products. Unambiguous determination of NMN and ATP concentrations in the nucleus, Golgi apparatus, and mitochondria is likely to be a technically challenging undertaking that is clearly beyond the scope of the present study. Another potentially useful approach would to assess the impact of exchanging the organelle-targeting sequences for each isozyme by molecular genetic techniques using human cell lines. In any case, we should stress that the underlying chemistry of these adenylyltransferases is unlikely to depend on whether one isozyme utilizes an ordered or a random kinetic mechanism, because the same nucleophilic reactions can occur once the EAB ternary complex is formed. Returning again to the example of creatine kinase, it is reasonable to assume that the same single in-line phosphoryl-transfer step occurs during conversion of Enz·ADP·Creatine-P into Enz·ATP·Creatine at both pH 7 or pH 8 (i.e., whether or not ADP and Creatine-P binding is ordered or random).

Because NMNAT is already regarded to be an important druggable target for cancer chemotherapy, there is justifiably great interest in developing high-affinity NMNAT inhibitors as lead molecules in drug development (*55*). In principle, the potency and isozyme-specific action of Np_3AD, Np_4AD, and Nap_4AD as multisubstrate geometric inhibitors can be improved by learning how these molecules are situated within the active sites of each. We and others have already undertaken extensive X-ray crystallographic studies of isozymes 1 and 3 (*24*, *56*−*58*), and it will be of interest to extend this work to binary complexes of the enzyme and the above dinucleotide inhibitors. Notably, although the adenylate kinase inhibitors Ap_4A and Ap_5A were originally thought to span the AMP and ATP subsites in the enzyme's catalytic center (*43*, *44*), later studies by Egner *et al.* (*59*) demonstrated that the enzyme cannot simultaneously bind both adenosine moieties of Ap_5A. Therefore, before attempting to improve the potency and specificity of these multisubstrate inhibitors, X-ray studies on the stereochemical arrangement of enzyme-bound Np_3AD, Np_4AD, and Nap_4AD are clearly indicated. Because the three NMNAT forms differ with respect to the interactions with nucleoside 5′-triphosphate substrate utilization, crystal studies and/or molecular dynamics modeling of Np_nAD, Np_nGD, and Np_nHD may also provide clues about how to achieve greater isozyme selectivity. Finally, because the individual NMNAT isozymes play distinctive roles in cellular physiology, the development of isozyme-specific multisubstrate inhibitors may prove to be invaluable in investigating NAD^+ biosynthesis in specific cell compartments.

Prior to this study, Northern blot analysis was the principal method for assessing the levels of the three NMNATs in cells. This indirect approach can be misleading, because the implicit assumption that the amount of enzyme parallels the cellular content of mRNA is not always valid. The unambiguous biochemical assay described in this report now permits us to determine the relative contribution of each NMNAT isozyme to NAD^+ biosynthesis in extracts of cell lines and tissues. The detailed kinetic studies underlying the above protocol led to the discovery of interesting issues, including the differential expression of the three isozymes within normal peritumoral tissues and related transformed cell lines.

ACKNOWLEDGMENT

We thank Profs. Silverio Ruggieri and Nadia Raffaelli for their helpful discussion during the preparation of the manuscript, and Dr. Lisa Pucci for her contribution in NMNAT cloning and real-time PCR analysis.

SUPPORTING INFORMATION AVAILABLE

Description of the primers used for cloning and the purification of the three recombinant NMNAT human isoforms. This material is available free of charge via the Internet at http://pubs.acs.org.

REFERENCES

1. Ueda, K., and Hayaishi, O. (1985) ADP-ribosylation, *Annu. Rev. Biochem. 54*, 73−100.
2. Germain, M., Scovassi, I., and Poirier, G. G. (2000) in *Cell Death: The Role of Poly(ADP-Ribose) Polymerase* (Szabo, C., Ed.) pp 209−225, CRC Press, Boca Raton, FL.
3. Clapper, D. L., Walseth, T. F., Dargle, P. J., and Lee, H. C. (1987) Pyridine nucleotide metabolites stimulate calcium release from

sea urchin egg microsomes desensitized to inositol trisphosphate, *J. Biol. Chem. 262*, 9561−9568.
4. Smith, S., Giriat, I., Schmitt, A., and de Lange, T. (1998) Tankyrase, a poly(ADP-ribose) polymerase at human telomeres, *Science 282*, 1484−1487.
5. Griffith, J. D., Comeau, L., Rosenfield, S., Stansel, R. M., Bianchi, A., Moss, H., and de Lange, T. (1999) Mammalian telomeres end in a large duplex loop, *Cell 97*, 503−514.
6. Imai, S. I., Armstrong, C. M., Kaeberlein, M., and Guarente, L. (2000) Transcriptional silencing and longevity protein Sir2 is an NAD-dependent histone deacetylase, *Nature 403*, 795−800.
7. Vaziri, H., Dessain, S. K., Ng Eaton, E., Imai, S. I., Frye, R. A., Pandita, T. K., Guarente, L., and Weinberg, R. A. (2001) hSIR2-(SIRT1) functions as an NAD-dependent p53 deacetylase, *Cell 107*, 149−159.
8. Luo, J., Nikolaev, A. Y., Imai, S., Chen, D., Su, F., Shiloh, A., Guarente, L., and Gu, W. (2001) Negative control of p53 by Sir2alpha promotes cell survival under stress, *Cell 107*, 137−148.
9. Adams, J. D., Klaidman, L. K., Ghang, M. L., and Yang, J. (2001) Brain oxidative stress-analytical chemistry and thermodynamics of glutathione and NADPH, *Curr. Top. Med. Chem. 1*, 473−482.
10. Magni, G., Amici, A., Emanuelli, M., Raffaelli, N., and Ruggieri, S. (1999) Enzymology of NAD^+ synthesis, *Adv. Enzymol. Relat. Areas Mol. Biol. 73*, 135−182.
11. Kaplan, N. O., Goldin, A, Humphreys, S. R., Ciotti, M. M., and Venditti, J. M. (1954) Significance of enzymatically catalyzed exchange reactions in chemotherapy, *Science 120*, 437−440.
12. Lamborg, M., Stolzenbach, F. E., and Kaplan, N. O. (1958) The nicotinic acid analogue of diphosphopyridine nucleotide, *J. Biol. Chem. 231*, 685−694.
13. Morton, R. K. (1958) Enzymic synthesis of coenzyme I in relation to chemical control of cell growth, *Nature 181*, 540−542.
14. Atkinson, M. R., Jackson, J. F., and Morton, R. K. (1961) Substrate specificity and inhibition of nicotinamide mononucleotideadenylyl transferase of liver nuclei: possible mechanism of effect of 6-mercaptopurine on tumour growth, *Nature 192*, 946−948.
15. Boulton, S., Kyle, S., and Durkacz, B. W. (1997) Low nicotinamide mononucleotide adenylyltransferase activity in a tiazofurin-resistant cell line: effects on NAD metabolism and DNA repair, *Br. J. Cancer 76*, 845−851.
16. Jayaram, H. N., Zhen, W., and Gharehbaghi, K. (1993) Biochemical consequences of resistance to tiazofurin in human myelogenous leukemic K562 cells, *Cancer Res. 53*, 2344−2348.
17. Jayaram, H. N., O'Connor, A., Grant, M. R., Yang, H, and Cooney, D. A. (1996) Biochemical consequences of resistance to a recently discovered IMP dehydrogenase inhibitor, benzamide riboside, in human myelogenous leukemia K562 cells, *J. Exp. Ther. Oncol. 1*, 278−285.
18. Bannwarth, H., and Siebert, G. (1969) Pyridine nucleotides in *Acetabularia mediterrranea* before and after removel of the cell nucleus, *Hoppe Seylers Z. Physiol. Chem. 350*, 1475−1476.
19. Kato, T., and Lowry, O. H. (1973) Distribution of enzymes between nucleus and cytoplasm of single nerve cell bodies, *J. Biol. Chem. 248*, 2044−2048.
20. Barile, M., Passarella, S., Danese, G., and Quagliariello, E. (1996) Rat liver mitochondria can synthesize nicotinamide adenine dinucleotide from nicotinamide mononucleotide and ATP via a putative matrix nicotinamide mononucleotide adenylyltransferase, *Biochem. Mol. Biol. Int. 38*, 297−306.
21. Emanuelli, M., Carnevali, F., Lorenzi, M., Raffaelli, N., Amici, A., Ruggieri, S., and Magni, G. (1999) Identification and characterization of YLR328W, the *Saccharomyces cerevisiae* structural gene encoding NMN adenylyltransferase. Expression and characterization of the recombinant enzyme, *FEBS Lett. 455*, 13−17.
22. Emanuelli, M., Amici, A., Carnevali, F., Pierella, F., Raffaelli, N., and Magni, G. (2003) Identification and characterization of a second NMN adenylyltransferase gene in *Saccharomyces cerevisiae*, *Protein Expression Purif. 27*, 357−364.
23. Magni, G., Amici, A., Emanuelli, M., Orsomando, G., Raffaelli, N., and Ruggieri, S. (2004) Enzymology of NAD^+ homeostasis in man, *Cell. Mol. Life Sci. 61*, 19−34.
24. Zhang, X., Kurnasov, O. V., Karthikeyan, S., Grishin, N. V., Osterman, A. L., and Zhang, H. (2003) Structural characterization of a human cytosolic NMN/NaMN adenylyltransferase and implication in human NAD biosynthesis, *J. Biol. Chem. 278*, 13503−13511.
25. Berger, F., Lau, C., Dahlmann, M., and Ziegler, M. (2005) Subcellular compartmentation and differential catalytic properties of the three human nicotinamide mononucleotide adenylyltransferase isoforms, *J. Biol. Chem. 280*, 36334−36341.
26. Magni, G., Amici, A., Emanuelli, M., Orsomando, G., Raffaelli, N., and Ruggieri, S. (2004) Structure and function of nicotinamide mononucleotide adenylyltransferase, *Curr. Med. Chem. 11*, 873−885.
27. Raffaelli, N., Sorci, L., Amici, A., Emanuelli, M., Mazzola, F., and Magni, G. (2002) Identification of a novel human nicotinamide mononucleotide adenylyltransferase, *Biochem. Biophys. Res. Commun. 297*, 835−840.
28. Sambrook, J., Fritsch, E. F., and Maniatis, T. (1989) in *Molecular Cloning: A Laboratory Manual*, 2nd ed., Cold Spring Harbor Laboratory, Cold Spring Harbor, NY.
29. Schägger, H., and Von Jagow, G. (1987) Tricine-sodium dodecyl sulfate-polyacrylamide gel electrophoresis for the separation of proteins in the range from 1 to 100 kDa, *Anal. Biochem. 166*, 368−379.
30. Balducci, E., Emanuelli, M., Raffaelli, N., Ruggieri, S., Amici, A., Magni, G., Orsomando, G., Polzonetti, V., and Natalini (1995) Assay methods for nicotinamide mononucleotide adenylyltransferase of wide applicability, *Anal. Biochem. 228*, 64−68.
31. Bradford, M. M. (1976) A rapid and sensitive method for the quantitation of microgram quantities of protein utilizing the principle of protein-dye binding, *Anal. Biochem. 72*, 248−254.
32. Franchetti, P., Cappellacci, L., Pasqualini, M., Grifantini, M., Lorenzi, T., Raffaelli, N., and Magni, G. (2003) Dinucleoside polyphosphate NAD analogs as potential NMN adenylyltransferase inhibitors. Synthesis and biological evaluation, *Nucleosides Nucleotides Nucleic Acids 22*, 865−868.
33. Cleland, W. W. (1977) Determining the chemical mechanisms of enzyme-catalyzed reactions by kinetic studies, *Adv. Enzymol. Relat. Areas Mol. Biol. 45*, 273−387.
34. Natalini, P., Ruggieri, S., Raffaelli, N., and Magni, G. (1986) Nicotinamide mononucleotide adenylyltransferase. Molecular and enzymatic properties of the homogeneous enzyme from baker's yeast, *Biochemistry 25*, 3725−3729.
35. Kolobe, D., Sayed, Y., and Dirr, H. W. (2004) Characterization of bromosulphophtalein binding to human glutathione S-transferase A1-1: thermodynamics and inhibition kinetics, *Biochem. J. 382*, 703−709.
36. Fromm, H. J. (1975) *Initial Rate Enzyme Kinetics*, Springer-Verlag, Berlin.
37. Arya, M., Shergill, I. S., Williamson, M., Gommersall, L., Arya, N., and Patel, H. R. (2005) Basic principles of real-time quantitative PCR, *Expert Rev. Mol. Diagn. 5*, 209−219.
38. Emanuelli, M., Natalini, P., Raffaelli, N., Ruggieri, S., Vita, A., and Magni, G. (1992) NAD biosynthesis in human placenta: purification and characterization of homogeneous NMN adenylyltransferase, *Arch. Biochem. Biophys. 298*, 29−34.
39. Balducci, E., Orsomando, G., Polzonetti, V., Vita, A., Emanuelli, M., Raffaelli, N., Ruggieri, S., Magni, G., and Natalini, P. (1995) NMN adenylyltransferase from bull testis: purification and properties, *Biochem. J. 310*, 395−400.
40. Rapizzi, E., Fossati, S., Moroni, F., and Chiarugi, A. (2004) Inhibition of poly(ADP-ribose) glycohydrolase by gallotannin selectively up-regulates expression of proinflammatory genes, *Mol. Pharmacol. 66*, 890−898.
41. McDougall, G. J., and Stewart, D. (2005) The inhibitory effects of berry polyphenols on digestive enzymes, *Biofactors 23*, 189−195.
42. Chung, K. T., Wong, T. Y., Wei, C. I., Huang, Y. W., and Lin, Y. (1998) Tannins and human health: a review, *Crit. Rev. Food Sci. Nutr. 38*, 421−464.
43. Purich, D. L., and Fromm, H. J. (1972) Inhibition of rabbit skeletal muscle adenylate kinase by the transition state analogue, P^1,P^4-di(adenosine-5′) tetraphosphate, *Biochim. Biophys. Acta 276*, 563−567.
44. Lienhard, G. E., and Secemski, I. I. (1973) P1,P5-Di(adenosine-5′)pentaphosphate, a potent multisubstrate inhibitor of adenylate kinase, *J. Biol. Chem. 248*, 1121−1123.
45. Sorci, L. (2000) Sintesi Enzimatica e Caratterizzazione di Nuovi Dinucleotidi Piridinici, *Laurea doctoral thesis* (Supervisor: Prof. G. Magni), Università degli Studi di Ancona.
46. Emanuelli, M., Carnevali, F., Pierella, F., Saccucci, F., Amici, A., Raffaelli, N., and Magni, G. (2000) Molecular and functional characterization of human recombinant NMN adenylyltransferase, *J. Biol. Regul. Homeostatic Agents 14*, 24−25.

47. Buniatian, G. K. h. (1975) Role of adenine mono- and dinucleotides in ammonia formation in brain tissue, *Vopr. Biokhim. Mozga 10*, 5−32.
48. Yalowitz, J. A., Xiao, S., Biju, M. P., Antony, A. C., Cummings, W. O., Deeg, M. A., and Jayaram, H. N. (2004) Characterization of human brain nicotinamide 5′-mononucleotide adenylyltransferase-2 and expression in human pancreas, *Biochem. J. 377*, 317−326.
49. Emanuelli, M., Carnevali, F., Saccucci, F., Pierella, F., Amici, A., Raffaelli, N., and Magni, G. (2001) Molecular cloning, chromosomal localization, tissue mRNA levels, bacterial expression, and enzymatic properties of human NMN adenylyltransferase, *J. Biol. Chem. 276*, 406−412.
50. Lee, J. S., and Thorgeirsson, S. S. (2002) Functional and genomic implications of global gene expression profiles in cell lines from human hepatocellular cancer, *Hepatology 35*, 1134−1143.
51. Wolfenden, R. (1969) Transition state analogues for enzyme catalysis, *Nature 223*, 704−705.
52. Wolfenden, R. (1972) Analog approaches to the structure of the transition state in enzyme reactions, *Acc. Chem. Res. 5*, 10−18.
53. Morrison, J. F., and James, E. (1965) *Biochem. J. 97*, 37−52.
54. Schimerlik, M. I., and Cleland, W. W. (1973) *J. Biol. Chem. 248*, 8418−8423.
55. Robertson, J. G. (2005) Mechanistic basis of enzyme-targeted drugs, *Biochemistry 44*, 5561−5571.
56. Garavaglia, S., D'Angelo, I., Emanuelli, M., Carnevali, F., Pierella, F., Magni, G., and Rizzi, M. (2002) Structure of human NMN adenylyltransferase. A key nuclear enzyme for NAD homeostasis, *J. Biol. Chem. 277*, 8524−8530.
57. Zhou, T., Kurnasov, O., Tomchick, D. R., Binns, D. D., Grishin, N. V., Marquez, V. E., Osterman, A. L., and Zhang, H. (2002) Structure of human nicotinamide/nicotinic acid mononucleotide adenylyltransferase. Basis for the dual substrate specificity and activation of the oncolytic agent tiazofurin, *J. Biol. Chem. 277*, 13148−13154.
58. Werner, E., Ziegler, M., Lerner, F., Schweiger, M., and Heinemann, U. (2002) Crystal structure of human nicotinamide mononucleotide adenylyltransferase in complex with NMN, *FEBS Lett. 516*, 239−244.
59. Egner, U., Tomasselli, A. G., and Schulz, G. E. (1987) Structure of the complex of yeast adenylate kinase with the inhibitor P1,-P5-di(adenosine-5′-)pentaphosphate at 2.6 Å resolution, *J. Mol. Biol. 195*, 649−658.

BI6023379